Refined 2D Models for the Analysis of Functionally Graded Piezoelectric Plates

S. Brischetto* and E. Carrera

Department of Aeronautics and Space Engineering, Politecnico di Torino, Italy

ABSTRACT: This article investigates the static analysis of a single-layered functionally graded piezoelectric plate, in both sensor and actuator configurations. Refined theories (order of expansion in the thickness direction from linear to fourth order) are compared with classical ones, such as the first order shear deformation theory, to demonstrate the effectiveness of these theories in the case of functionally graded piezoelectric materials (FGPMs). Both elastic and electrical properties in FGPMs are described via opportune thickness functions, which are a combination of Legendre polynomials, with an order of expansion in thickness direction equal to 10. Such types of functions permit any functional variation of the FGPM properties to be described efficiently in the thickness direction.

Key Words: Carrera's unified formulation, principle of virtual displacements, functionally graded materials, piezoelectric materials, actuator configuration, sensor configuration.

INTRODUCTION

Functionally graded materials (FGMs) can be utilized to provide the desired thermomechanical, piezoelectric, and magnetic properties, via the spatial variation in their composition. FGMs can be applied in several fields, including tribology, electronics, biomechanics, aeronautics, and space research. The special feature of graded spatial compositions associated with FGMs provides freedom in the design and manufacturing of novel structures; on the other hand, it also poses great challenges in numerical modeling and simulation of the FGM structures (Pan and Han, 2005a; He et al., 2007). Embedding a network of piezoceramic actuators and sensors in FGM structures creates a self-controlling and self-monitoring smart system. This newly engineered class of materials has resulted in significant improvements in the performance of integrated systems, actuation technologies, shape control, vibration and acoustic control, and condition monitoring (Liew et al., 2004). An alternative solution could be the use of piezoelectric materials, functionally graded in the thickness direction (FGPM), in order to build smart structures which are extensively used as sensors and actuators (Li et al., 2008). The development of piezoelectric materials and structures with FGPM properties along the layer-thickness direction, to improve the mechanical and electrical properties at layer interfaces, has received increasing attention in recent years (Lu et al., 2006). Most of the studies on FGPM laminates are based on 2D plate theories and for this reason analytical 3D solutions are useful. They can exactly predict the mechanical and electrical behavior. Among these, the following works are of particular interest. Lu et al. (2006) presented an alternative method for the derivation of exact solutions of a simply supported, rectangular, functionally graded piezoelectric plate or laminate. In this approach, the related equations and formulas are developed in terms of an elegant formalism that is similar to the Stroh formalism. A similar derivation of exact solutions was proposed by the same authors for the case of cylindrical bending (Lu et al., 2005). Pan and Han (2005b) offered an exact solution for a multilayered rectangular plate made of functionally graded, anisotropic, and linear magneto-electro-elastic materials. The edges of the plate are under simply supported conditions and the FGM is assumed to be exponential in the thickness direction. The 3D solution given by Ootao and Tanigawa (2000) concerns a transient piezothermoelasticity problem developed for a functionally graded rectangular plate bonded to a piezoelectric plate and subjected to a partial heat supply. Zhong and Shang (2003) proposed an exact 3D solution for a functionally graded piezoelectric rectangular plate that is simply supported and grounded along its four edges. The plate is under mechanical and/or electric loading on the upper and lower surfaces. A new formulation for exact solutions of the system, based on the Euler-Bernoulli theory, was presented in Joshi et al. (2003) for the case of an active FGM subjected to electrical excitation. The structure is

*Author to whom correspondence should be addressed.
E-mail: salvatore.brischetto@polito.it
Figures 1 and 2 appear in color online: http://jim.sagepub.com

1045-389X/09/15 1783–15 $10.00/0 DOI: 10.1177/1045389X08098444

comprised of a substrate, an electro-elastically graded layer, and an active layer.

The above 3D solutions can provide benchmark results to assess the accuracy of 2D plate theories and numerical methods. In the case of FGPMs, classical theories are not effective in obtaining the mechanical and electrical variables, but high order theories and advanced models are necessary for this purpose. Almajid et al. (2001) gave a modified classical lamination theory (CLT) to analyze piezoelectric coupling terms under an applied electric field. A standard piezoelectric bimorph and a newly proposed piezoelectric graded microstructure bimorph were analyzed using this CLT. Another modified CLT was applied by Takagi et al. (2003), to verify an FGM actuator. A weak form formulation, based on the first order shear deformation theory (FSDT), was established by Dai et al. (2005) for active shape control as well as the dynamic response repression of a FGM plate containing piezoelectric sensors and actuators. Static and dynamic responses are presented in He et al. (2001) for FGM plates with integrated piezoelectric sensors and actuators. A finite element formulation, based on the classical lamination plate theory, is considered. A refinement of classical theories was proposed in Wu et al. (2002) to examine the electromechanical behavior of generic piezoelectric shells with graded material properties in the thickness direction. By means of a high order theory, it is possible to obtain governing equations that can be readily reduced to typical structures, such as beams, plates, and circular cylindrical shells. An interesting numerical investigation was proposed by Bhangale and Ganesan (2006) for the static analysis of functionally graded, anisotropic, and linear magneto-electro-elastic plates. A series solution is assumed in the plane of the plate and a finite element procedure is adopted across the thickness of the plate. The present finite element is modeled with displacement components, and with electric potential and magnetic potential as nodal degrees of freedom. The other fields are calculated by post-processing via constitutive equations. An alternative FE solution was proposed in Ray and Sachade (2006) for the case of an FGM plate with Young's modulus varying exponentially along the thickness direction, and integrated with a layer of piezoelectric fiber-reinforced composite. The buckling of piezoelectric FGM rectangular plates subjected to non-uniformly distributed loads, heat, and voltage was analyzed by Chen et al. (2008) using a free Galerkin (EFG) method. The free vibration problem for these types of structures was analyzed in Chen and Ding (2002). In this case, separation formulae for displacements and shear stresses are employed.

This article presents a compact and generalized formulation for plates that includes functionally graded piezoelectric layers. To this aim, Carrera's unified formulation (CUF) (Carrera, 1995, 2003) successfully extended to functionally graded plates in Brischetto and Carrera (2008), Brischetto et al. (2008), and Carrera et al. (2008), is now adapted to smart structures including FGPMs. The extension to electromechanical coupling in the case of plates including classical piezoelectric layers was made in Carrera and Boscolo (2007), Carrera and Brischetto (2007), and Ballhause et al. (2005). Only single-layered FGPM plates in sensor and actuator configurations are considered in the present work, to verify the effectiveness of this new formulation. Multilayered smart structures, including FGPM layers, will be investigated in future works. The principle of virtual displacements (PVD) for the electromechanical case is employed to derive governing equations. The thickness varying material properties are addressed by means of higher order models, where the three displacement components and the electric potential can be considered with different orders of expansion in the thickness direction (from linear to fourth order). Classical theories, such as FSDT, have been added to the investigation for comparison purposes. FSDT can be obtained thanks to the CUF via a penalty technique. The article is organized as follows: the second section extends the CUF to FGMs, the third gives the opportune geometrical and constitutive equations. The governing equations are obtained in the fourth section in the framework of PVD application. The fifth section discusses the proposed results in the case of single-layered FGPM plates. Finally, the conclusions are addressed in the last section.

CARRERA'S UNIFIED FORMULATION

The application of a 2D method for plates permits the unknown variables to be expressed in a set of thickness functions that only depend on the thickness coordinate z and the correspondent variable that depends on the in-plane coordinates (x, y).

CUF (Carrera, 1995) is a technique that handles a large variety of plate/shell modelings in a unified manner. Therefore, the generic variable $\boldsymbol{a}(x, y, z)$, for instance a displacement, and its variation $\delta\boldsymbol{a}(x, y, z)$ are written according to the following general expansion:

$$\begin{aligned} \boldsymbol{a}(x, y, z) &= F_\tau(z)\boldsymbol{a}_\tau(x, y) \\ \delta\boldsymbol{a}(x, y, z) &= F_s(z)\delta\boldsymbol{a}_s(x, y) \\ \text{with } \tau, s &= 1, \ldots, N \end{aligned} \tag{1}$$

where the bold letters denote arrays, (x, y) are the in-plane coordinates, and z the thickness coordinate. The summing convention, with repeated indexes τ and s, is assumed.

Equation (1) could be used for the primary variables, which, in the case of an electromechanical problem,

are the displacement components $\boldsymbol{u}$ and the electric potential Φ, and to describe the variation of the elastic and electric properties through the thickness direction in the case of a FGPM.

CUF for the Primary Variables

For a 2D model based on PVD (Carrera, 2003), in the case of an electromechanical coupling, the primary variables are the displacement components $\boldsymbol{u} = (u_x, u_y, u_z)$ and the electric potential Φ. In the case of a single-layered plate, these variables can be described along the thickness via a Taylor expansion:

$$\begin{aligned} &\boldsymbol{u}(x,y,z) = F_\tau(z)\boldsymbol{u}_\tau(x,y) \\ &\delta\boldsymbol{u}(x,y,z) = F_s(z)\delta\boldsymbol{u}_s(x,y) \\ &\Phi(x,y,z) = F_\tau(z)\Phi_\tau(x,y) \\ &\delta\Phi(x,y,z) = F_s(z)\delta\Phi_s(x,y) \\ &\text{with } \tau, s = 1,\ldots,N. \end{aligned} \tag{2}$$

The thickness functions are the terms of the Taylor expansion:

$$F_\tau(z) = F_s(z) = z^N \quad \text{with } N = 0,1,2,3,4. \tag{3}$$

Several higher order models can be obtained, from $N=1$ to $N=4$, depending the chosen order of expansion in z. For example, the $N=2$ model reads:

$$\begin{aligned} u_x(x,y,z) &= 1\,u_{x0}(x,y) + z u_{x1}(x,y) + z^2 u_{x2}(x,y) \\ u_y(x,y,z) &= 1\,u_{y0}(x,y) + z u_{y1}(x,y) + z^2 u_{y2}(x,y) \\ u_z(x,y,z) &= 1\,u_{z0}(x,y) + z u_{z1}(x,y) + z^2 u_{z2}(x,y) \\ \Phi(x,y,z) &= 1\Phi_0(x,y) + z\Phi_1(x,y) + z^2\Phi_2(x,y). \end{aligned} \tag{4}$$

The FSDT can be obtained as particular case of the $N=1$ model, imposing a constant transverse displacement u_z through the thickness direction z.

Extension of CUF to FGPMs

In case of a FGPM, the properties can change with continuity in the plate along a particular direction. In the present article, mechanical and electrical properties vary with continuity along the thickness direction z. The matrices of elastic coefficients $\boldsymbol{C}$, piezoelectric coefficients $\boldsymbol{e}$, and dielectric coefficients $\boldsymbol{\varepsilon}$ are assumed as in the following:

$$\begin{aligned} \boldsymbol{C}(z) &= \boldsymbol{C}_0 * f(z) \\ \boldsymbol{e}(z) &= \boldsymbol{e}_0 * g(z) \\ \boldsymbol{\varepsilon}(z) &= \boldsymbol{\varepsilon}_0 * h(z). \end{aligned} \tag{5}$$

The functions $f(z)$, $g(z)$, and $h(z)$ are general continuous functions of the thickness coordinate z. The variation in z of these material properties can be described via particular thickness functions, which are a combination of Legendre polynomials (Carrera et al., 2008):

$$\begin{aligned} \boldsymbol{C}(z) &= F_\mathrm{b}(z)\boldsymbol{C}_\mathrm{b} + F_\gamma(z)\boldsymbol{C}_\gamma + F_\mathrm{t}(z)\boldsymbol{C}_\mathrm{t} = F_r\boldsymbol{C}_r \\ \boldsymbol{e}(z) &= F_\mathrm{b}(z)\boldsymbol{e}_\mathrm{b} + F_\gamma(z)\boldsymbol{e}_\gamma + F_\mathrm{t}(z)\boldsymbol{e}_\mathrm{t} = F_r\boldsymbol{e}_r \\ \boldsymbol{\varepsilon}(z) &= F_\mathrm{b}(z)\boldsymbol{\varepsilon}_\mathrm{b} + F_\gamma(z)\boldsymbol{\varepsilon}_\gamma + F_\mathrm{t}(z)\boldsymbol{\varepsilon}_\mathrm{t} = F_r\boldsymbol{\varepsilon}_r. \end{aligned} \tag{6}$$

t and b are the top and bottom values, and γ terms denote the higher order terms of expansion. The thickness functions $F_r(\zeta_k)$ have now been defined at the k-layer level; they are a linear combination of Legendre polynomials $P_j = P_j(\zeta_k)$ of the j-th order defined in ζ_k-domain ($\zeta_k = (2z_k)/(h_k)$ with z_k local coordinate and h_k thickness, both referred to k-th layer, so $-1 \le \zeta_k \le 1$). For example, the first five Legendre polynomials are:

$$\begin{aligned} &P_0 = 1,\ P_1 = \zeta_k,\ P_2 = \frac{(3{\zeta_k}^2 - 1)}{2}, \\ &P_3 = \frac{5{\zeta_k}^3}{2} - \frac{3\zeta_k}{2},\ P_4 = \frac{35{\zeta_k}^4}{8} - \frac{15{\zeta_k}^2}{4} + \frac{3}{8}. \end{aligned} \tag{7}$$

Their combinations for the thickness functions are:

$$\begin{aligned} &F_\mathrm{t} = \frac{P_0 + P_1}{2},\ F_\mathrm{b} = \frac{P_0 - P_1}{2}, \\ &F_\gamma = P_\gamma - P_{\gamma-2} \quad \text{with } \gamma = 2,\ldots,10. \end{aligned} \tag{8}$$

In the present article a value of r equal to 10 has been chosen, which always guarantees a good approximation of the FGPM properties. To obtain the $\boldsymbol{C}_r$, $\boldsymbol{e}_r$, and $\boldsymbol{\varepsilon}_r$ values, it is sufficient to solve a simple algebraic system as shown in Equation (9):

$$\begin{bmatrix} (C_{ij}, e_{ij}, \varepsilon_{ij})(z_1) \\ \vdots \\ (C_{ij}, e_{ij}, \varepsilon_{ij})(z_{N_r}) \end{bmatrix} = \begin{bmatrix} F_\mathrm{b}(z_1) & \cdots & F_\gamma(z_1) & \cdots & F_\mathrm{t}(z_1) \\ \vdots & & \vdots & & \vdots \\ F_\mathrm{b}(z_{N_r}) & \cdots & F_\gamma(z_{N_r}) & \cdots & F_\mathrm{t}(z_{N_r}) \end{bmatrix} \begin{bmatrix} C_{ijb}, e_{ijb}, \varepsilon_{ijb} \\ \vdots \\ C_{ij\gamma}, e_{ij\gamma}, \varepsilon_{ij\gamma} \\ \vdots \\ C_{ijt}, e_{ijt}, \varepsilon_{ijt} \end{bmatrix}. \tag{9}$$

The values of $C(z)$, $e(z)$, and $\varepsilon(z)$, and the thickness functions $F_r(z)$ are known in 10 different locations along the thickness of the plate. By solving the system in Equation (9), the values C_r, e_r, and ε_r are obtained. The material properties varying with continuity in the thickness direction z can be recovered, as illustrated in Equation (10) and in Figure 1:

$$\begin{aligned}(\boldsymbol{C}_{pp}(z), \boldsymbol{C}_{pn}(z), \boldsymbol{C}_{np}(z), \boldsymbol{C}_{nn}(z)) \\ = F_r(\boldsymbol{C}_{ppr}, \boldsymbol{C}_{pnr}, \boldsymbol{C}_{npr}, \boldsymbol{C}_{nnr}) \\ (\boldsymbol{e}_p(z), \boldsymbol{e}_n(z)) = F_r(\boldsymbol{e}_{pr}, \boldsymbol{e}_{nr}) \\ (\boldsymbol{\varepsilon}(z)) = F_r(\boldsymbol{\varepsilon}_r).\end{aligned} \tag{10}$$

The forms and dimensions of the matrices indicated in Equation (10) are:

$$\boldsymbol{C} = \begin{bmatrix} C_{11} & C_{12} & C_{16} & 0 & 0 & C_{13} \\ C_{12} & C_{22} & C_{26} & 0 & 0 & C_{23} \\ C_{16} & C_{26} & C_{66} & 0 & 0 & C_{63} \\ 0 & 0 & 0 & C_{55} & C_{45} & 0 \\ 0 & 0 & 0 & C_{45} & C_{44} & 0 \\ C_{31} & C_{32} & C_{36} & 0 & 0 & C_{33} \end{bmatrix} = \begin{bmatrix} \mathbf{C}_{pp} & \mathbf{C}_{pn} \\ \mathbf{C}_{np} & \mathbf{C}_{nn} \end{bmatrix}. \tag{11}$$

$$\mathbf{e}_p = \begin{bmatrix} 0 & 0 & 0 \\ 0 & 0 & 0 \\ e_{31} & e_{32} & e_{36} \end{bmatrix} \quad \mathbf{e}_n = \begin{bmatrix} e_{15} & e_{14} & 0 \\ e_{25} & e_{24} & 0 \\ 0 & 0 & e_{33} \end{bmatrix}$$

$$\boldsymbol{\varepsilon} = \begin{bmatrix} \varepsilon_{11} & \varepsilon_{12} & 0 \\ \varepsilon_{21} & \varepsilon_{22} & 0 \\ 0 & 0 & \varepsilon_{33} \end{bmatrix}. \tag{12}$$

GEOMETRICAL RELATIONS AND CONSTITUTIVE EQUATIONS

This section illustrates the geometrical relations for a piezoelectric plate, and the constitutive equations for the application of the PVD to electromechanical problems in case of FGPMs.

Geometrical Relations

In-plane $\boldsymbol{\varepsilon_p}$ and out-plane strains $\boldsymbol{\varepsilon_n}$ can be related to displacements $\boldsymbol{u} = (u_x, u_y, u_z)$, and electric field $\boldsymbol{\mathcal{E}}$ is related to electric potential Φ by means of geometrical

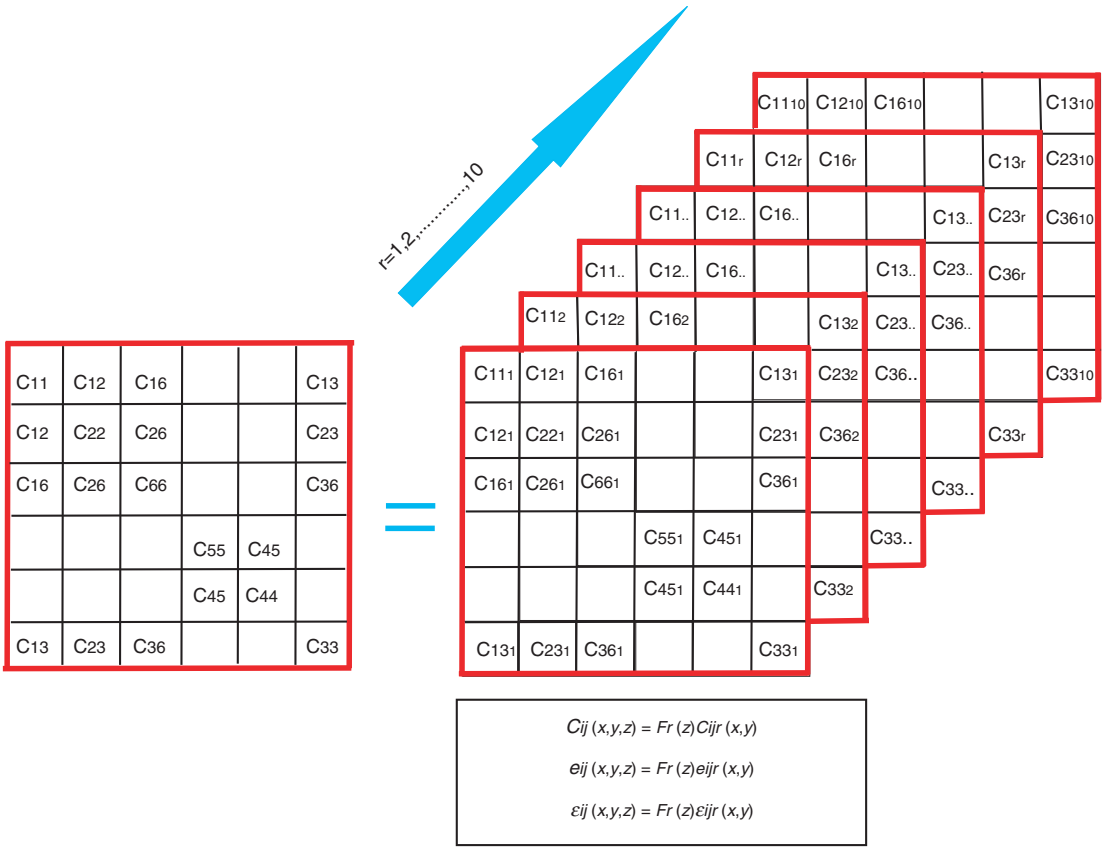

Figure 1. *Example of assembling on index r for the FGPM properties.*

relations; in the case of plates these relations (subscript G) assume the following differential forms:

$$\begin{aligned}\boldsymbol{\varepsilon}_{pG} &= [\varepsilon_{xx}, \varepsilon_{yy}, \varepsilon_{xy}]^T = \boldsymbol{D}_p \boldsymbol{u} \\ \boldsymbol{\varepsilon}_{nG} &= [\varepsilon_{xz}, \varepsilon_{yz}, \varepsilon_{zz}]^T = (\boldsymbol{D}_{n\Omega} + \boldsymbol{D}_{nz})\, \boldsymbol{u} \\ \boldsymbol{\mathcal{E}}_G &= [\mathcal{E}_x, \mathcal{E}_y, \mathcal{E}_z]^T = -(\boldsymbol{D}_{e\Omega} + \boldsymbol{D}_{ez})\, \Phi.\end{aligned} \tag{13}$$

The explicit form of the introduced arrays follows:

$$\begin{aligned}\boldsymbol{D}_p &= \begin{bmatrix} \partial_x & 0 & 0 \\ 0 & \partial_y & 0 \\ \partial_y & \partial_x & 0 \end{bmatrix} \quad \boldsymbol{D}_{n\Omega} = \begin{bmatrix} 0 & 0 & \partial_x \\ 0 & 0 & \partial_y \\ 0 & 0 & 0 \end{bmatrix} \\ \boldsymbol{D}_{nz} &= \begin{bmatrix} \partial_z & 0 & 0 \\ 0 & \partial_z & 0 \\ 0 & 0 & \partial_z \end{bmatrix} \quad \boldsymbol{D}_{e\Omega} = \begin{bmatrix} \partial_x \\ \partial_y \\ 0 \end{bmatrix} \quad \boldsymbol{D}_{ez} = \begin{bmatrix} 0 \\ 0 \\ \partial_z \end{bmatrix}.\end{aligned} \tag{14}$$

Constitutive Equations

In case of an electromechanical problem, if we consider a FGPM, the constitutive equations link the in-plane stresses $\boldsymbol{\sigma}_p = (\sigma_{xx}, \sigma_{yy}, \sigma_{xy})$, the out-plane stresses $\boldsymbol{\sigma}_n = (\sigma_{xz}, \sigma_{yz}, \sigma_{zz})$ and the electric displacement $\boldsymbol{\mathcal{D}} = (\mathcal{D}_x, \mathcal{D}_y, \mathcal{D}_z)$ to strains $\boldsymbol{\varepsilon}$ and the electric field $\boldsymbol{\mathcal{E}}$ (Carrera and Boscolo, 2007; Carrera and Brischetto, 2007). The constitutive equations are identified via the subscript C, and are considered for each layer k. In case of FGPMs, the coefficients depend on the thickness coordinate z:

$$\begin{aligned}\boldsymbol{\sigma}_{pC}^k &= \boldsymbol{C}_{pp}^k(z)\boldsymbol{\varepsilon}_{pG}^k + \boldsymbol{C}_{pn}^k(z)\boldsymbol{\varepsilon}_{nG}^k - \boldsymbol{e}_p^{k^T}(z)\boldsymbol{\mathcal{E}}_G^k \\ \boldsymbol{\sigma}_{nC}^k &= \boldsymbol{C}_{np}^k(z)\boldsymbol{\varepsilon}_{pG}^k + \boldsymbol{C}_{nn}^k(z)\boldsymbol{\varepsilon}_{nG}^k - \boldsymbol{e}_n^{k^T}(z)\boldsymbol{\mathcal{E}}_G^k \\ \boldsymbol{\mathcal{D}}_C^k &= \boldsymbol{e}_p^k(z)\boldsymbol{\varepsilon}_{pG}^k + \boldsymbol{e}_n^k(z)\boldsymbol{\varepsilon}_{nG}^k + \boldsymbol{\varepsilon}^k(z)\boldsymbol{\mathcal{E}}_G^k.\end{aligned} \tag{15}$$

If in Equation (15), we consider the description in z illustrated in Equation (10), we obtain the constitutive equations in case of FGPMs:

$$\begin{aligned}\boldsymbol{\sigma}_{pC}^k &= F_r\boldsymbol{C}_{ppr}^k\boldsymbol{\varepsilon}_{pG}^k + F_r\boldsymbol{C}_{pnr}^k\boldsymbol{\varepsilon}_{nG}^k - F_r\boldsymbol{e}_{pr}^{k^T}\boldsymbol{\mathcal{E}}_G^k \\ \boldsymbol{\sigma}_{nC}^k &= F_r\boldsymbol{C}_{npr}^k\boldsymbol{\varepsilon}_{pG}^k + F_r\boldsymbol{C}_{nnr}^k\boldsymbol{\varepsilon}_{nG}^k - F_r\boldsymbol{e}_{nr}^{k^T}\boldsymbol{\mathcal{E}}_G^k \\ \boldsymbol{\mathcal{D}}_C^k &= F_r\boldsymbol{e}_{pr}^k\boldsymbol{\varepsilon}_{pG}^k + F_r\boldsymbol{e}_{nr}^k\boldsymbol{\varepsilon}_{nG}^k + F_r\boldsymbol{\varepsilon}_r^k\boldsymbol{\mathcal{E}}_G^k.\end{aligned} \tag{16}$$

An additional loop on index r is considered in case of FGPMs, as described by the thickness functions F_r in Equation (16) and by the scheme illustrated in Figure 1. In case of 'classical' piezoelectric materials the elastic and piezoelectric coefficients are constant in z, so the further thickness functions F_r are not requested.

GOVERNING EQUATIONS

In case of electromechanical coupling the PVD, for a multilayered FGPM plate state:

$$\begin{aligned}&\sum_{k=1}^{N_l}\int_{\Omega_k}\int_{A_k}\left\{\delta\boldsymbol{\varepsilon}_{pG}^{k\,T}\boldsymbol{\sigma}_{pC}^k + \delta\boldsymbol{\varepsilon}_{nG}^{k\,T}\boldsymbol{\sigma}_{nC}^k - \delta\boldsymbol{\mathcal{E}}_G^{k\,T}\boldsymbol{\mathcal{D}}_C^k\right\} \\ &\qquad \mathrm{d}\Omega_k\,\mathrm{d}z = \delta L_{\mathrm{e}} + \delta L_{\mathrm{in}}\end{aligned} \tag{17}$$

where k indicates the k-th layer, N_l the number of layers, Ω_k and A_k are the integration domains in in-plane and thickness directions, respectively. δL_{e} is the external virtual work and δL_{in} is the virtual work made by the inertial forces. The first step is the substitution of the constitutive equations indicated in Equation (16) and the geometrical relations of Equation (13), so for a general layer k it is possible to write:

$$\begin{aligned}&\int_{\Omega_k}\int_{A_k}\Big\{(\boldsymbol{D}_p\delta\boldsymbol{u}^k)^T\Big[\Big(F_r\boldsymbol{C}_{ppr}^k\boldsymbol{D}_p + F_r\boldsymbol{C}_{pnr}^k(\boldsymbol{D}_{n\Omega}+\boldsymbol{D}_{nz})\Big)\boldsymbol{u}^k \\ &\quad + F_r\boldsymbol{e}_{pr}^{k^T}(\boldsymbol{D}_{e\Omega}+\boldsymbol{D}_{ez})\Phi^k\Big] + ((\boldsymbol{D}_{n\Omega}+\boldsymbol{D}_{nz})\delta\boldsymbol{u}^k)^T \\ &\quad \Big[\Big(F_r\boldsymbol{C}_{npr}^k\boldsymbol{D}_p + F_r\boldsymbol{C}_{nnr}^k(\boldsymbol{D}_{n\Omega}+\boldsymbol{D}_{nz})\Big)\boldsymbol{u}^k \\ &\quad + F_r\boldsymbol{e}_{nr}^{k^T}(\boldsymbol{D}_{e\Omega}+\boldsymbol{D}_{ez})\Phi^k\Big] + ((\boldsymbol{D}_{e\Omega}+\boldsymbol{D}_{ez})\delta\Phi^k)^T \\ &\quad \Big[\Big(F_r\boldsymbol{e}_{pr}^k\boldsymbol{D}_p + F_r\boldsymbol{e}_{nr}^k(\boldsymbol{D}_{n\Omega}+\boldsymbol{D}_{nz})\Big)\boldsymbol{u}^k \\ &\quad + F_r\boldsymbol{\varepsilon}_r^k(\boldsymbol{D}_{e\Omega}+\boldsymbol{D}_{ez})\Phi^k\Big]\Big\}\mathrm{d}\Omega_k\,\mathrm{d}z = \delta L_{\mathrm{e}}^k + \delta L_{\mathrm{in}}^k.\end{aligned} \tag{18}$$

After, we can introduce the CUF as just illustrated in Equation (2):

$$\begin{aligned}&\int_{\Omega_k}\int_{A_k}\Big\{(\boldsymbol{D}_p\delta\boldsymbol{u}_s^k)^T F_s\Big[\Big(F_r\boldsymbol{C}_{ppr}^k\boldsymbol{D}_p + F_r\boldsymbol{C}_{pnr}^k(\boldsymbol{D}_{n\Omega}+\boldsymbol{D}_{nz})\Big)F_\tau\boldsymbol{u}_\tau^k \\ &\quad + F_r\boldsymbol{e}_{pr}^{k^T}(\boldsymbol{D}_{e\Omega}+\boldsymbol{D}_{ez})F_\tau\Phi_\tau^k\Big] + ((\boldsymbol{D}_{n\Omega}+\boldsymbol{D}_{nz})\delta\boldsymbol{u}_s^k)^T F_s \\ &\quad \Big[\Big(F_r\boldsymbol{C}_{npr}^k\boldsymbol{D}_p + F_r\boldsymbol{C}_{nnr}^k(\boldsymbol{D}_{n\Omega}+\boldsymbol{D}_{nz})\Big)F_\tau\boldsymbol{u}_\tau^k \\ &\quad + F_r\boldsymbol{e}_{nr}^{k^T}(\boldsymbol{D}_{e\Omega}+\boldsymbol{D}_{ez})F_\tau\Phi_\tau^k\Big] + ((\boldsymbol{D}_{e\Omega}+\boldsymbol{D}_{ez})\delta\Phi_s^k)^T F_s \\ &\quad \Big[\Big(F_r\boldsymbol{e}_{pr}^k\boldsymbol{D}_p + F_r\boldsymbol{e}_{nr}^k(\boldsymbol{D}_{n\Omega}+\boldsymbol{D}_{nz})\Big)F_\tau\boldsymbol{u}_\tau^k \\ &\quad + F_r\boldsymbol{\varepsilon}_r^k(\boldsymbol{D}_{e\Omega}+\boldsymbol{D}_{ez})F_\tau\Phi_\tau^k\Big]\Big\}\mathrm{d}\Omega_k\,\mathrm{d}z = \delta L_{\mathrm{e}}^k + \delta L_{\mathrm{in}}^k.\end{aligned} \tag{19}$$

Now, we can apply the integration by parts using Gauss theorem to move the derivatives from virtual variations, which means:

$$\int_{\Omega_k} \left(\boldsymbol{D}_\xi \delta \boldsymbol{a}^k\right)^T \boldsymbol{a}^k \, \mathrm{d}\Omega_k = -\int_{\Omega_k} \delta \boldsymbol{a}^{kT} \boldsymbol{D}_\xi^T \boldsymbol{a}^k \, \mathrm{d}\Omega_k + \int_{\Gamma_k} \delta \boldsymbol{a}^{kT} \boldsymbol{I}_\xi^T \boldsymbol{a}^k \, \mathrm{d}\Gamma_k \tag{20}$$

with $\xi = p,\ n\Omega,\ e\Omega$ and $\boldsymbol{a} = \boldsymbol{u},\ \Phi$. For the boundary Γ_k the following matrices are considered:

$$\boldsymbol{I}_p = \begin{bmatrix} 1 & 0 & 0 \\ 0 & 1 & 0 \\ 1 & 1 & 0 \end{bmatrix}, \quad \boldsymbol{I}_{n\Omega} = \begin{bmatrix} 0 & 0 & 1 \\ 0 & 0 & 1 \\ 0 & 0 & 0 \end{bmatrix} \text{ e } \boldsymbol{I}_{e\Omega} = \begin{bmatrix} 1 \\ 1 \\ 0 \end{bmatrix}. \tag{21}$$

After integration by parts, the governing equation states:

$$\begin{aligned}
&\int_{\Omega_k}\int_{A_k} \Big\{ \delta \boldsymbol{u}_s^{kT}(-\boldsymbol{D}_p^T) F_s \Big[\Big(F_r \boldsymbol{C}_{ppr}^k \boldsymbol{D}_p + F_r \boldsymbol{C}_{pnr}^k (\boldsymbol{D}_{n\Omega} + \boldsymbol{D}_{nz}) \Big) F_\tau \boldsymbol{u}_\tau^k \\
&+ F_r \boldsymbol{e}_{pr}^{kT} (\boldsymbol{D}_{e\Omega} + \boldsymbol{D}_{ez}) F_\tau {\Phi_\tau}^k \Big] + \delta \boldsymbol{u}_s^{kT} (-\boldsymbol{D}_{n\Omega}^T + \boldsymbol{D}_{nz}^T) F_s \\
&\Big[\Big(F_r \boldsymbol{C}_{npr}^k \boldsymbol{D}_p + F_r \boldsymbol{C}_{nnr}^k (\boldsymbol{D}_{n\Omega} + \boldsymbol{D}_{nz}) \Big) F_\tau \boldsymbol{u}_\tau^k \\
&+ F_r \boldsymbol{e}_{nr}^{kT} (\boldsymbol{D}_{e\Omega} + \boldsymbol{D}_{ez}) F_\tau {\Phi_\tau}^k \Big] + \delta \Phi_s^{kT} (-\boldsymbol{D}_{e\Omega}^T + \boldsymbol{D}_{ez}^T) F_s \\
&\Big[\Big(F_r \boldsymbol{e}_{pr}^k \boldsymbol{D}_p + F_r \boldsymbol{e}_{nr}^k (\boldsymbol{D}_{n\Omega} + \boldsymbol{D}_{nz}) \Big) F_\tau \boldsymbol{u}_\tau^k \\
&+ F_r \boldsymbol{\varepsilon}_r^k (\boldsymbol{D}_{e\Omega} + \boldsymbol{D}_{ez}) F_\tau {\Phi_\tau}^k \Big] \Big\} \mathrm{d}\Omega_k \, \mathrm{d}z + \\
&\int_{\Gamma_k}\int_{A_k} \Big\{ \delta \boldsymbol{u}_s^{kT} \boldsymbol{I}_p^T F_s \Big[\Big(F_r \boldsymbol{C}_{ppr}^k \boldsymbol{D}_p + F_r \boldsymbol{C}_{pnr}^k (\boldsymbol{D}_{n\Omega} + \boldsymbol{D}_{nz}) \Big) F_\tau \boldsymbol{u}_\tau^k \\
&+ F_r \boldsymbol{e}_{pr}^{kT} (\boldsymbol{D}_{e\Omega} + \boldsymbol{D}_{ez}) F_\tau {\Phi_\tau}^k \Big] + \delta \boldsymbol{u}_s^{kT} \boldsymbol{I}_{n\Omega}^T F_s \\
&\Big[\Big(F_r \boldsymbol{C}_{npr}^k \boldsymbol{D}_p + F_r \boldsymbol{C}_{nnr}^k (\boldsymbol{D}_{n\Omega} + \boldsymbol{D}_{nz}) \Big) F_\tau \boldsymbol{u}_\tau^k \\
&+ F_r \boldsymbol{e}_{nr}^{kT} (\boldsymbol{D}_{e\Omega} + \boldsymbol{D}_{ez}) F_\tau {\Phi_\tau}^k \Big] + \delta \Phi_s^{kT} \boldsymbol{I}_{e\Omega}^T F_s \\
&\Big[\Big(F_r \boldsymbol{e}_{pr}^k \boldsymbol{D}_p + F_r \boldsymbol{e}_{nr}^k (\boldsymbol{D}_{n\Omega} + \boldsymbol{D}_{nz}) \Big) F_\tau \boldsymbol{u}_\tau^k \\
&+ F_r \boldsymbol{\varepsilon}_r^k (\boldsymbol{D}_{e\Omega} + \boldsymbol{D}_{ez}) F_\tau {\Phi_\tau}^k \Big] \Big\} \mathrm{d}\Omega_k \, \mathrm{d}z = \delta L_{\mathrm{e}}^k + \delta L_{\mathrm{in}}^k.
\end{aligned} \tag{22}$$

The governing equations can be written as:

$$\begin{aligned}
\delta \boldsymbol{u}_s^k &: \boldsymbol{K}_{uu}^{k\tau sr} \boldsymbol{u}_\tau^k + \boldsymbol{K}_{u\Phi}^{k\tau sr} \Phi_\tau^k = \boldsymbol{p}_{u\tau}^k \\
\delta \Phi_s^k &: \boldsymbol{K}_{\Phi u}^{k\tau sr} \boldsymbol{u}_\tau^k + \boldsymbol{K}_{\Phi\Phi}^{k\tau sr} \Phi_\tau^k = \boldsymbol{p}_{\Phi\tau}^k.
\end{aligned} \tag{23}$$

The arrays $\boldsymbol{p}_{u\tau}^k$ and $\boldsymbol{p}_{\Phi\tau}^k$ indicate the variationally consistent mechanical and electric loadings, respectively.

Along with these governing equations, the following boundary conditions on the edge Γ_k of the in-plane integration domain Ω_k hold:

$$\begin{aligned}
&\boldsymbol{u}_\tau^k = \bar{\boldsymbol{u}}_\tau^k \ \textit{or}\ \boldsymbol{\Pi}_{uu}^{k\tau sr} \boldsymbol{u}_\tau^k + \boldsymbol{\Pi}_{u\Phi}^{k\tau sr} \Phi_\tau^k = \boldsymbol{\Pi}_{uu}^{k\tau sr} \bar{\boldsymbol{u}}_\tau^k + \boldsymbol{\Pi}_{u\Phi}^{k\tau sr} \bar{\Phi}_\tau^k \\
&\Phi_\tau^k = \bar{\Phi}_\tau^k \ \textit{or}\ \boldsymbol{\Pi}_{\Phi u}^{k\tau sr} \boldsymbol{u}_\tau^k + \boldsymbol{\Pi}_{\Phi\Phi}^{k\tau sr} \Phi_\tau^k = \boldsymbol{\Pi}_{\Phi u}^{k\tau sr} \bar{\boldsymbol{u}}_\tau^k + \boldsymbol{\Pi}_{\Phi\Phi}^{k\tau sr} \bar{\Phi}_\tau^k.
\end{aligned} \tag{24}$$

Comparing Equation (22) with Equation (23), the explicit form of the fundamental nuclei can be obtained:

$$\begin{aligned}
\boldsymbol{K}_{uu}^{k\tau sr} = \int_{A_k} \Big\{ &- \boldsymbol{D}_p^T (\boldsymbol{C}_{ppr}^k F_\tau F_s F_r \boldsymbol{D}_p + \boldsymbol{C}_{pnr}^k F_\tau F_s F_r \boldsymbol{D}_{n\Omega} \\
&+ \boldsymbol{C}_{pnr}^k F_\tau F_s F_r \boldsymbol{D}_{nz}) + (\boldsymbol{D}_{nz}^T - \boldsymbol{D}_{n\Omega}^T) \\
&(\boldsymbol{C}_{npr}^k F_\tau F_s F_r \boldsymbol{D}_p + \boldsymbol{C}_{nnr}^k F_\tau F_s F_r \boldsymbol{D}_{n\Omega} \\
&+ \boldsymbol{C}_{nnr}^k F_\tau F_s F_r \boldsymbol{D}_{nz}) \Big\} \mathrm{d}z
\end{aligned} \tag{25}$$

$$\begin{aligned}
\boldsymbol{K}_{u\Phi}^{k\tau sr} = \int_{A_k} \Big\{ &- \boldsymbol{D}_p^T (\boldsymbol{e}_{pr}^{kT} F_\tau F_s F_r \boldsymbol{D}_{ez} + \boldsymbol{e}_{pr}^{kT} F_\tau F_s F_r \boldsymbol{D}_{e\Omega}) \\
&+ (\boldsymbol{D}_{nz}^T - \boldsymbol{D}_{n\Omega}^T) (\boldsymbol{e}_{nr}^{kT} F_\tau F_s F_r \boldsymbol{D}_{ez} + \boldsymbol{e}_{nr}^{kT} F_\tau F_s F_r \boldsymbol{D}_{e\Omega}) \Big\} \mathrm{d}z
\end{aligned} \tag{26}$$

$$\begin{aligned}
\boldsymbol{K}_{\Phi u}^{k\tau sr} = \int_{A_k} \Big\{ &(\boldsymbol{D}_{ez}^T - \boldsymbol{D}_{e\Omega}^T) (\boldsymbol{e}_{pr}^k F_\tau F_s F_r \boldsymbol{D}_p \\
&+ \boldsymbol{e}_{nr}^k F_\tau F_s F_r \boldsymbol{D}_{nz} + \boldsymbol{e}_{nr}^k F_\tau F_s F_r \boldsymbol{D}_{n\Omega}) \Big\} \mathrm{d}z
\end{aligned} \tag{27}$$

$$\begin{aligned}
\boldsymbol{K}_{\Phi\Phi}^{k\tau sr} = \int_{A_k} \Big\{ &(-\boldsymbol{D}_{e\Omega}^T + \boldsymbol{D}_{ez}^T) (\boldsymbol{\varepsilon}_r^k F_\tau F_s F_r \boldsymbol{D}_{ez} \\
&+ \boldsymbol{\varepsilon}_r^k F_\tau F_s F_r \boldsymbol{D}_{e\Omega}) \Big\} \mathrm{d}z.
\end{aligned} \tag{28}$$

The nuclei for boundary conditions on edge Γ_k are:

$$\begin{aligned}
\boldsymbol{\Pi}_{uu}^{k\tau sr} = \int_{A_k} \Big\{ &\boldsymbol{I}_p^T (\boldsymbol{C}_{ppr}^k F_\tau F_s F_r \boldsymbol{D}_p + \boldsymbol{C}_{pnr}^k F_\tau F_s F_r \boldsymbol{D}_{n\Omega} \\
&+ \boldsymbol{C}_{pnr}^k F_\tau F_s F_r \boldsymbol{D}_{nz}) + \boldsymbol{I}_{n\Omega}^T (\boldsymbol{C}_{npr}^k F_\tau F_s F_r \boldsymbol{D}_p \\
&+ \boldsymbol{C}_{nnr}^k F_\tau F_s F_r \boldsymbol{D}_{n\Omega} + \boldsymbol{C}_{nnr}^k F_\tau F_s F_r \boldsymbol{D}_{nz}) \Big\} \mathrm{d}z
\end{aligned} \tag{29}$$

$$\begin{aligned}
\boldsymbol{\Pi}_{u\Phi}^{k\tau sr} = \int_{A_k} \Big\{ &\boldsymbol{I}_p^T (\boldsymbol{e}_{pr}^{kT} F_\tau F_s F_r \boldsymbol{D}_{ez} + \boldsymbol{e}_{pr}^{kT} F_\tau F_s F_r \boldsymbol{D}_{e\Omega}) \\
&+ \boldsymbol{I}_{n\Omega}^T (\boldsymbol{e}_{nr}^{kT} F_\tau F_s F_r \boldsymbol{D}_{ez} + \boldsymbol{e}_{nr}^{kT} F_\tau F_s F_r \boldsymbol{D}_{e\Omega}) \Big\} \mathrm{d}z
\end{aligned} \tag{30}$$

$$\begin{aligned}
\boldsymbol{\Pi}_{\Phi u}^{k\tau sr} = \int_{A_k} \Big\{ &\boldsymbol{I}_{e\Omega}^T (\boldsymbol{e}_{pr}^k F_\tau F_s F_r \boldsymbol{D}_p + \boldsymbol{e}_{nr}^k F_\tau F_s F_r \boldsymbol{D}_{nz} \\
&+ \boldsymbol{e}_{nr}^k F_\tau F_s F_r \boldsymbol{D}_{n\Omega}) \Big\} \mathrm{d}z
\end{aligned} \tag{31}$$

$$\boldsymbol{\Pi}_{\Phi\Phi}^{k\tau sr} = \int_{A_k} \Big\{ \boldsymbol{I}_{e\Omega}^T (\boldsymbol{\varepsilon}_r^k F_\tau F_s F_r \boldsymbol{D}_{ez} + \boldsymbol{\varepsilon}_r^k F_\tau F_s F_r \boldsymbol{D}_{e\Omega}) \Big\} \mathrm{d}z. \tag{32}$$

The indexes indicated in the fundamental nuclei are used for the assembling procedure, as illustrated in the recent authors' papers (Brischetto and Carrera, 2008; Brischetto et al., 2008; Carrera et al., 2008). The index r represents the assembling for the FGMs properties (Figure 1); it is not considered in case of 'classical' materials. The indexes τ and s are the assembling for the chosen order of expansion of the primary variables in the thickness direction. The index k represents the multilayer assembling procedure in case of multilayer structures. In the present case it is not considered because we investigate only single-layered plates. The multilayer assembling procedure on index k in both equivalent single-layered and layer-wise overviews has just been detailed in Brischetto and Carrera (2008) and Carrera et al. (2008).

The explicit form of fundamental nuclei, in closed form solution are reported in the Appendix.

RESULTS AND DISCUSSION

In order to verify the effectiveness of the proposed advanced models as well as to evaluate their performance with respect to FSDT, the benchmark proposed by Lu et al. (2006) is considered. A single-layered FGPM simply supported plate is investigated. This is a functionally graded piezoelectric plate that has the PZT-4 as a reference material:

$$C_{11}^0 = C_{22}^0 = 139\,\text{GPa} \qquad C_{33}^0 = 115\,\text{GPa}$$
$$C_{12}^0 = 77.8\,\text{GPa} \qquad C_{13}^0 = C_{23}^0 = 74.3\,\text{GPa}$$
$$C_{44}^0 = C_{55}^0 = 25.6\,\text{GPa} \qquad C_{66}^0 = 30.6\,\text{GPa}$$
$$e_{31}^0 = e_{32}^0 = -5.2\,\text{C/m}^2 \qquad e_{33}^0 = 15.1\,\text{C/m}^2$$
$$e_{51}^0 = e_{42}^0 = 12.7\,\text{C/m}^2 \qquad \varepsilon_{11}^0 = \varepsilon_{22}^0 = 1.306 \times 10^{-8}\,\text{F/m}$$
$$\varepsilon_{33}^0 = 1.151 \times 10^{-8}\,\text{F/m}.$$

These properties change in the thickness direction z according to the following law:

$$\boldsymbol{C}(z) = \boldsymbol{C}^0 \exp^{\beta \frac{z}{h}}$$
$$\boldsymbol{e}(z) = \boldsymbol{e}^0 \exp^{\beta \frac{z}{h}} \tag{33}$$
$$\boldsymbol{\varepsilon}(z) = \varepsilon^0 \exp^{\beta \frac{z}{h}}$$

with $0 < z < h$ and $-1.0 < \beta < 1.0$. h is the thickness of the plate and the in-plane plate dimensions are $a = b = 1\,\text{m}$. Each variable considered in the tables and figures is investigated in $x = y = 0.25a$.

Lu et al. (2006) gave an exact 3D solution for two possible configurations, as illustrated in Figure 2. The sensor configuration has a mechanical load applied at the top:

$$P_z^t = \bar{P}_z \sin\left(\frac{m\pi x}{a}\right) \sin\left(\frac{n\pi y}{b}\right)$$
$$\Phi^{\text{t}} = \Phi^{\text{b}} = 0 \tag{34}$$

with $m = n = 1$ and $\bar{P}_z = -1$.

The actuator configuration has an electric potential applied at the top:

$$\Phi^{\text{t}} = \bar{\Phi}_z \sin\left(\frac{m\pi x}{a}\right) \sin\left(\frac{n\pi y}{b}\right)$$
$$\Phi^{\text{b}} = 0 \tag{35}$$

with $m = n = 1$ and $\bar{\Phi} = 1$. t and b mean the top and bottom of the plate, respectively. m and n are the chosen wavenumbers in the plane. The 3D solutions by Lu et al. (2006) were unfortunately only given in graphic form and, as a consequence, only a few significant digits are considered in the tables.

Tables 1–3 consider the sensor configuration for thin and very thin plates. Mechanical and electrical variables are investigated for different values of the parameter β (which means different thickness laws for the material properties, $\beta = 0$ means 'classical' PZT-4). To obtain the 3D solutions, higher orders of

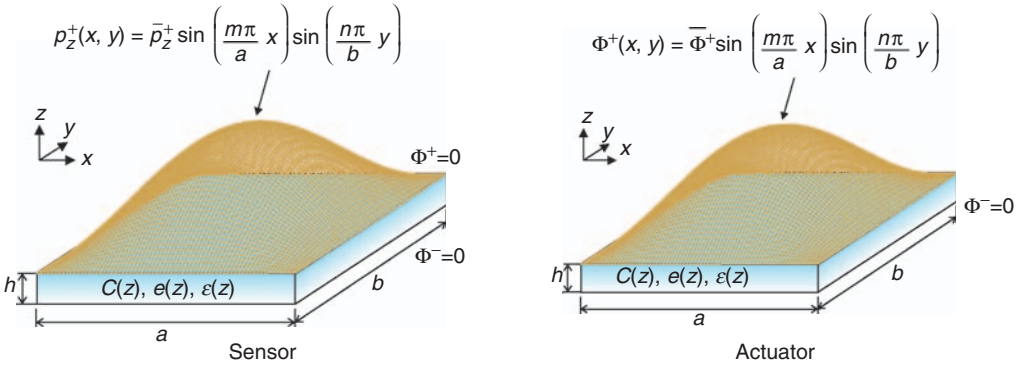

Figure 2. *Example of a single-layered functionally graded piezoelectric plate in sensor and actuator configuration.*

Table 1. Sensor configuration. In-plane and transverse displacements u_x and u_z in $h=0$ and $x=y=0.25$. Moderately thick and thin plates. Three-dimensional solution by Lu et al. (2006).

	$h=0.1$				$h=0.01$			
β	3D	$N=4$	$N=2$	FSDT	3D	$N=4$	$N=2$	FSDT
		u_x10^{-11}				u_x10^{-9}		
−1.0	0.650	0.647	0.650	0.463	–	0.695	0.695	0.462
−0.5	0.247	0.243	0.245	0.185	–	0.280	0.280	0.185
0.0	−0.031	−0.029	−0.029	0.000	–	0.000	0.000	0.000
0.5	−0.197	−0.192	−0.193	−0.112	–	−0.170	−0.170	−0.112
1.0	−0.275	−0.273	−0.274	−0.170	–	−0.256	−0.256	−0.170
		u_z10^{-9}				u_z10^{-6}		
−1.0	−0.251	−0.248	−0.247	−0.197	–	−0.237	−0.237	−0.182
−0.5	−0.196	−0.194	−0.193	−0.154	–	−0.184	−0.184	−0.142
0.0	−0.151	−0.151	−0.150	−0.121	–	−0.143	−0.143	−0.111
0.5	−0.119	−0.118	−0.117	−0.094	–	−0.112	−0.112	−0.086
1.0	−0.094	−0.092	−0.092	−0.072	–	−0.087	−0.087	−0.067

Table 2. Sensor configuration. Electric potential Φ and electric displacement $\mathcal{D}_z$ in $h=0$ and $x=y=0.25$. Moderately thick and thin plates. Three-dimensional solution by Lu et al. (2006).

	$h=0.1$				$h=0.01$			
β	3D	$N=4$	$N=2$	FSDT	3D	$N=4$	$N=2$	FSDT
		$\Phi10^{-2}$				$\Phi10^{-1}$		
−1.0	−0.596	−0.591	−0.592	0.000	–	−0.588	−0.590	0.000
−0.5	−0.492	−0.493	−0.492	0.000	–	−0.490	−0.490	0.000
0.0	−0.393	−0.393	−0.392	0.000	–	−0.390	−0.390	0.000
0.5	−0.299	−0.299	−0.298	0.000	–	−0.297	−0.297	0.000
1.0	−0.220	−0.217	−0.218	0.000	–	−0.216	−0.217	0.000
		$\mathcal{D}_z10^{-9}$				$\mathcal{D}_z10^{-7}$		
−1.0	0.312	0.316	0.323	0.091	–	0.379	0.395	0.091
−0.5	0.144	0.142	0.139	0.050	–	0.202	0.204	0.047
0.0	−0.061	−0.059	−0.059	0.000	–	−0.001	−0.001	0.000
0.5	−0.267	−0.259	−0.259	−0.047	–	−0.203	−0.205	−0.047
1.0	−0.445	−0.432	−0.444	−0.091	–	−0.380	−0.396	−0.091

Table 3. Sensor configuration. In-plane stresses $\sigma_{xx}(-h/2)$, $\sigma_{xy}(+h/2)$ and transverse normal stress $\sigma_{zz}(+h/2)$ in $x=y=0.25$. Moderately thick and thin plates. Three-dimensional solution by Lu et al. (2006).

	$h=0.1$				$h=0.01$			
β	3D	$N=4$	$N=2$	FSDT	3D	$N=4$	$N=2$	FSDT
		σ_{xx}				σ_{xx}		
−1.0	15.23	15.21	15.22	16.33	–	1509	1505	1631
−0.5	13.05	12.97	12.94	13.95	–	1286	1286	1395
0.0	10.92	10.96	10.88	11.85	–	1088	1088	1185
0.5	9.138	9.156	9.042	9.989	–	909.1	909.4	998.7
1.0	7.529	7.504	7.401	8.323	–	745.5	748.2	831.6
		σ_{xy}				$\sigma_{xy}10^3$		
−1.0	3.041	3.039	3.011	2.347	–	0.312	0.312	0.235
−0.5	3.616	3.612	3.581	2.818	–	0.370	0.370	0.282
0.0	4.247	4.241	4.207	3.345	–	0.432	0.432	0.334
0.5	4.959	4.952	4.917	3.937	–	0.502	0.502	0.394
1.0	5.830	5.773	5.739	4.604	–	0.582	0.582	0.460
		σ_{zz}				σ_{zz}		
−1.0	−0.500	−0.511	−0.385	5.700	−0.500	−0.511	−0.381	−570.0
−0.5	−0.500	−0.507	−0.445	−6.846	−0.500	−0.507	−0.441	−684.6
0.0	−0.500	−0.500	−0.516	−8.125	−0.500	−0.500	−0.512	−812.5
0.5	−0.500	−0.491	−0.596	−9.563	−0.500	−0.490	−0.593	−956.3
1.0	−0.500	−0.481	−0.681	−11.18	−0.500	−0.480	−0.679	−1118

expansion are requested. FSDT gives very large errors with respect to the 3D model. Considering the variation of the parameter β, when this is different from zero, the electric potential is never linear even if the plate is thin. The FSDT considers the electric potential linear and this introduces a further error in the analysis of FGM plates. For thin plates, the $N=2$ model gives quite good results, but for thick plates, as illustrated in Table 4, the use of the $N=4$ model is mandatory. For particular variables, such as the transverse normal stress σ_{zz} and the transverse-normal electric displacement $\mathcal{D}_z$, the use of the $N=4$ model is mandatory even if the plate is thin, as shown in Tables 2 and 3. In the case of a sensor configuration, it is not possible to obtain the electric potential Φ by means of FSDT, because the degrees of freedom of this theory are not sufficient to impose the short-circuit configuration ($\Phi^t = \Phi^b = 0$). Using the $N=4$ model, it is possible to obtain the quasi-3D evaluation for any value of the thickness h and the parameter β. The variables plotted in Figure 3 are for thickness $h=0.1$ and for each value of β. The results given by the $N=4$ model are in agreement with the 3D solution in Lu et al. (2006). The plots in Figures 4 and 5 clearly demonstrate the inefficiency of the FSDT model; the $N=4$ and $N=2$ models are very close for the thin plate ($h=0.01$).

The comments made for the sensor configuration are also confirmed for the actuator case. The same variables of the sensor case are investigated for the actuator in Tables 5–8. It is clearly shown in Figure 6 that for particular variables, such as the transverse shear/normal stresses σ_{xz} and σ_{zz}, even when a higher order model is applied, the results are not completely satisfactory. The zero-homogeneous conditions for σ_{xz} and σ_{zz} at the top and bottom of the plate are difficult to reach. A possible remedy to this situation could be the extension of Reissner's Mixed Variational Theorem (RMVT) to FGPM plates, in which case, the transverse shear/normal stresses are considered as independent variables and evaluated *a priori*. Figures 7 and 8 confirm the inadequacy of the FSDT for these types of problem.

CONCLUSIONS

In this article, CUF has been extended to FGPM plates in the framework of the PVD. Refined models with higher orders of expansion in the thickness direction have been implemented; FSDT results have been obtained as particular cases. Thickness functions, obtained as combinations of Legendre polynomials, have been introduced to describe the variation of the material properties in the thickness direction. The use of advanced models (higher orders of expansion) is mandatory for FGPM plates, as the FSDT is inefficient for such structures. Future developments could be devoted to the analysis of multilayered plates including FGPM layers, as well as the use of the RMVT to *a priori* obtain some transverse variables such as the transverse shear/normal stresses $\boldsymbol{\sigma}_n$ and the normal electric displacement $\mathcal{D}_z$.

Table 4. Sensor configuration. Transverse displacement $u_z(0)$, electric potential $\Phi(0)$, and transverse normal stress $\sigma_{zz}(+h/2)$ in $x=y=0.25$. Thick plates. Three-dimensional solution by Lu et al. (2006).

	$h=0.25$				$h=0.15$			
β	3D	$N=4$	$N=2$	FSDT	3D	$N=4$	$N=2$	FSDT
		$u_z 10^{-10}$				$u_z 10^{-10}$		
−1.0	−0.200	−0.196	−0.189	−0.177	−0.780	−0.777	−0.767	−0.639
−0.5	−0.157	−0.156	−0.151	−0.141	−0.615	−0.611	−0.602	−0.504
0.0	−0.124	−0.124	−0.120	−0.111	−0.480	−0.479	−0.471	−0.394
0.5	−0.098	−0.098	−0.094	−0.085	−0.375	−0.375	−0.369	−0.306
1.0	−0.078	−0.076	−0.074	−0.065	−0.294	−0.293	−0.289	−0.235
		$\Phi 10^{-2}$				$\Phi 10^{-2}$		
−1.0	–	−0.242	−0.240	0.000	–	−0.396	−0.396	0.000
−0.5	–	−0.202	−0.199	0.000	–	−0.331	−0.329	0.000
0.0	–	−0.161	−0.159	0.000	–	−0.263	−0.262	0.000
0.5	–	−0.122	−0.121	0.000	–	−0.200	−0.200	0.000
1.0	–	−0.088	−0.088	0.000	–	−0.146	−0.146	0.000
		σ_{zz}				σ_{zz}		
−1.0	−0.500	−0.511	−0.405	−0.912	−0.500	−0.511	−0.390	−2.533
−0.5	−0.500	−0.508	−0.464	−1.095	−0.500	−0.507	−0.450	−3.042
0.0	−0.500	−0.501	−0.532	−1.300	−0.500	−0.500	−0.520	−3.611
0.5	−0.500	−0.492	−0.608	−1.530	−0.500	−0.491	−0.599	−4.250
1.0	−0.500	−0.483	−0.688	−1.789	−0.500	−0.481	−0.682	−4.970

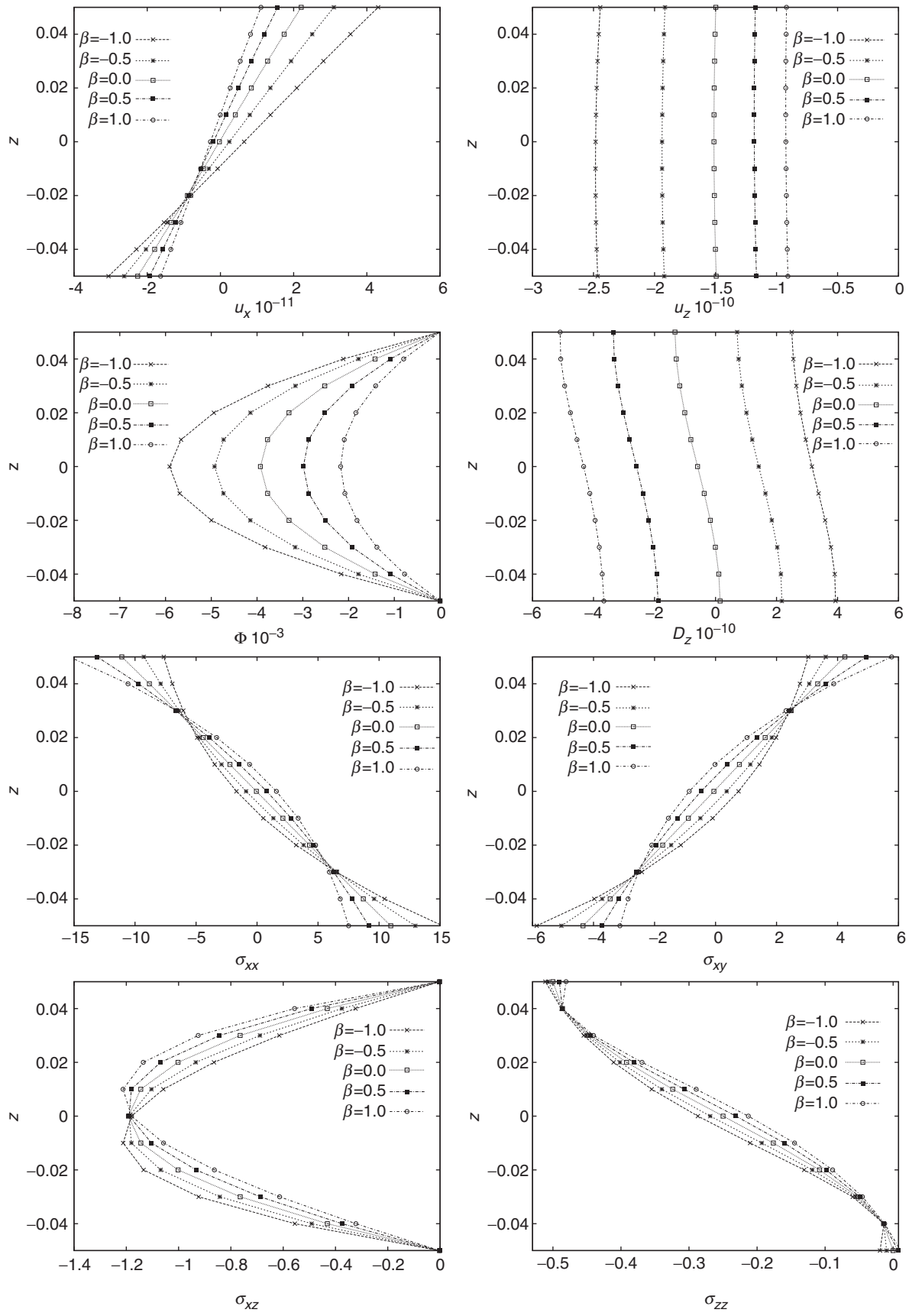

Figure 3. *Functionally graded piezoelectric plate with thickness $h = 0.1$. Sensor configuration, $N = 4$ model. Three-dimensional solution by Lu et al. (2006).*

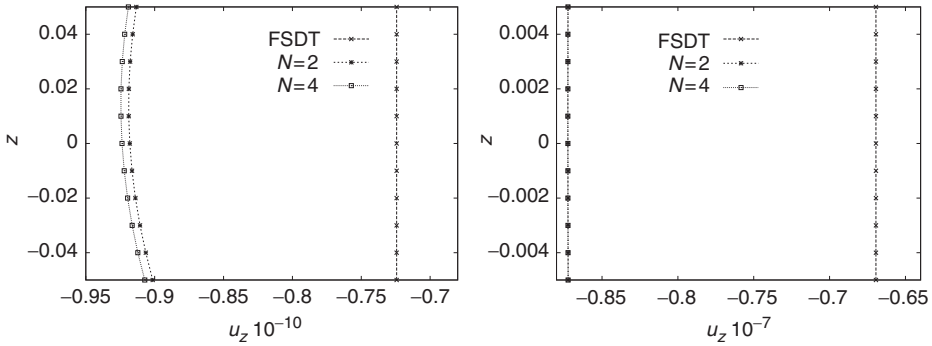

Figure 4. *Functionally graded piezoelectric plate with thickness h = 0.1 (left) and h = 0.01(right). Sensor configuration N = 4, N = 2, and FSDT models. Exponential β = 1.0.*

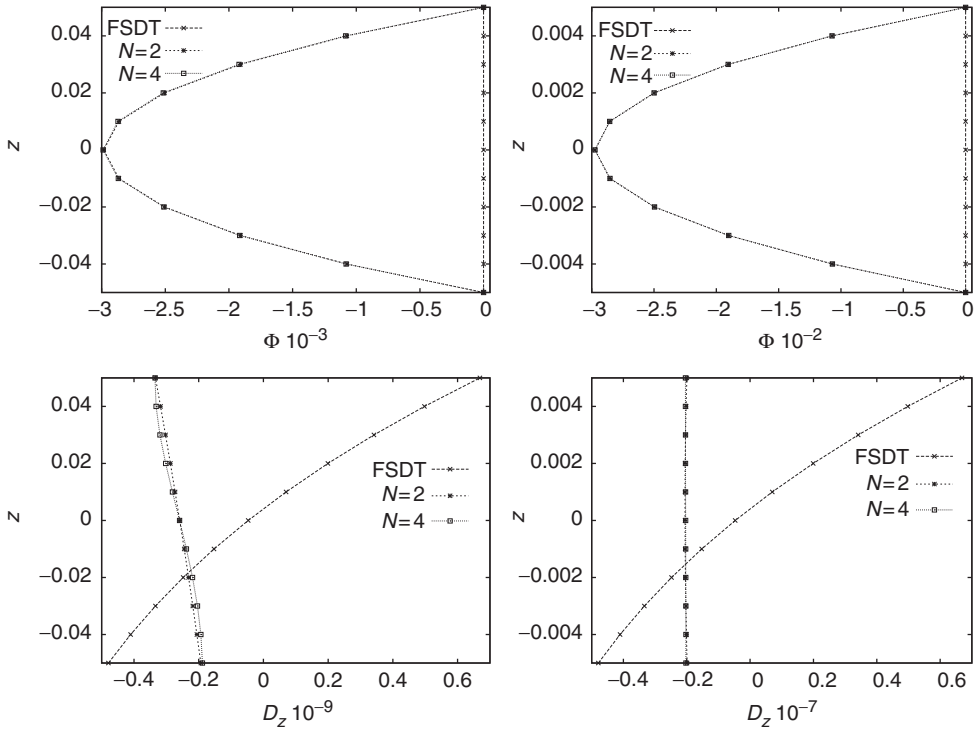

Figure 5. *Functionally graded piezoelectric plate with thickness h = 0.1 (left) and h = 0.01 (right). Sensor configuration, N = 4, N = 2, and FSDT models. Exponential β = 0.5.*

Table 5. Actuator configuration. In-plane and transverse displacements u_x and u_z in h = 0 and x = y = 0.25. Moderately thick and thin plates. Three-dimensional solution by Lu et al. (2006).

	h = 0.1				**h = 0.01**			
β	**3D**	**N = 4**	**N = 2**	**FSDT**	**3D**	**N = 4**	**N = 2**	**FSDT**
		u_x10^{-9}				u_x10^{-8}		
−1.0	−0.129	−0.125	−0.125	−0.029	–	−0.126	−0.126	−0.029
−0.5	−0.129	−0.128	−0.128	−0.030	–	−0.129	−0.129	−0.030
0.0	−0.129	−0.128	−0.129	−0.030	–	−0.130	−0.130	−0.030
0.5	−0.129	−0.128	−0.128	−0.030	–	−0.129	−0.129	−0.030
1.0	−0.129	−0.125	−0.125	−0.029	–	−0.126	−0.126	−0.029
		u_z10^{-9}				u_z10^{-7}		
−1.0	0.327	0.325	0.323	−0.101	–	0.379	0.379	−0.002
−0.5	0.140	0.139	0.138	−0.113	–	0.202	0.202	−0.001
0.0	−0.074	−0.072	−0.072	−0.124	–	−0.001	−0.001	−0.001
0.5	−0.280	−0.283	−0.282	−0.133	–	−0.204	−0.204	−0.001
1.0	−0.480	−0.466	−0.466	−0.137	–	−0.380	−0.381	0.000

Table 6. Actuator configuration. Electric potential Φ and electric displacement $\mathcal{D}_z$ in $h=0$ and $x=y=0.25$. Moderately thick and thin plates. Three-dimensional solution by Lu et al. (2006).

	$h=0.1$				$h=0.01$			
β	3D	$N=4$	$N=2$	FSDT	3D	$N=4$	$N=2$	FSDT
		Φ				Φ		
−1.0	0.181	0.183	0.185	0.250	–	0.188	0.190	0.250
−0.5	0.210	0.212	0.213	0.250	–	0.219	0.219	0.250
0.0	0.242	0.243	0.243	0.250	–	0.250	0.250	0.250
0.5	0.272	0.273	0.273	0.250	–	0.281	0.281	0.250
1.0	0.300	0.303	0.301	0.250	–	0.311	0.309	0.250
		$\mathcal{D}_z 10^{-7}$				$\mathcal{D}_z 10^{-6}$		
−1.0	−0.457	−0.455	−0.481	−0.355	–	−0.461	−0.481	−0.355
−0.5	−0.609	−0.606	−0.619	−0.456	–	−0.613	−0.619	−0.456
0.0	−0.787	−0.788	−0.796	−0.585	–	−0.796	−0.796	−0.585
0.5	−1.009	−1.004	−1.021	−0.751	–	−1.011	−1.021	−0.751
1.0	−1.257	−1.249	−1.306	−0.965	–	−1.253	−1.307	−0.965

Table 7. Actuator configuration. In-plane stresses $\sigma_{xx}(-h/2)$, $\sigma_{xy}(+h/2)$ and transverse normal stress $\sigma_{zz}(+h/2)$ in $x=y=0.25$. Moderately thick and thin plates. Three-dimensional solution by Lu et al. (2006).

	$h=0.1$				$h=0.01$			
β	3D	$N=4$	$N=2$	FSDT	3D	$N=4$	$N=2$	FSDT
		σ_{xx}				σ_{xx}		
−1.0	−18.06	−18.04	−10.81	−5.862	–	−187.3	−135.9	−59.58
−0.5	−19.71	−19.71	−15.79	−5.766	–	−206.3	−190.5	−57.97
0.0	−23.79	−23.68	−21.29	−5.722	–	−250.2	−250.0	−57.22
0.5	−31.75	−31.75	−27.49	−5.791	–	−337.7	−316.5	−58.34
1.0	−44.27	−45.61	−34.62	−6.063	–	−486.5	−393.2	−62.50
		σ_{xy}				σ_{xy}		
−1.0	−14.22	−13.80	−13.79	−2.050	–	−131.5	−131.7	−20.50
−0.5	−20.31	−19.99	−19.97	−3.452	–	−188.0	−188.0	−34.52
0.0	−27.19	−27.16	−27.15	−5.722	–	−250.6	−250.6	−57.22
0.5	−34.84	−34.56	−36.56	−9.399	–	−309.2	−309.3	−93.99
1.0	−41.72	−41.00	−41.04	−15.37	–	−348.8	−349.3	−153.7
		σ_{zz}				σ_{zz}		
−1.0	0.000	0.002	0.611	32.75	0.000	0.000	0.063	327.5
−0.5	0.000	0.003	0.995	54.18	0.000	0.000	0.102	541.8
0.0	0.000	0.005	1.545	89.40	0.000	0.000	0.159	894.0
0.5	0.000	0.008	2.316	147.3	0.000	0.000	0.238	1473
1.0	0.000	0.001	3.426	242.6	0.000	−0.002	0.351	2426

Table 8. Actuator configuration. Transverse displacement $u_z(0)$, electric potential $\Phi(0)$ and transverse normal stress $\sigma_{zz}(+h/2)$ in $x=y=0.25$. Thick plates. Three-dimensional solution by Lu et al. (2006).

	$h=0.25$				$h=0.15$			
β	3D	$N=4$	$N=2$	FSDT	3D	$N=4$	$N=2$	FSDT
		$u_z 10^{-9}$				$u_z 10^{-9}$		
−1.0	–	0.013	0.011	−0.100	–	0.116	0.114	−0.100
−0.5	–	−0.023	−0.024	−0.113	–	0.029	0.027	−0.113
0.0	–	−0.063	−0.064	−0.124	–	−0.070	−0.070	−0.124
0.5	–	−0.102	−0.102	−0.133	–	−0.167	−0.167	−0.133
1.0	–	−0.136	−0.137	−0.139	–	−0.252	−0.252	−0.138
		Φ				Φ		
−1.0	0.159	0.159	0.163	0.250	0.176	0.177	0.180	0.250
−0.5	0.184	0.184	0.185	0.250	0.203	0.205	0.206	0.250
0.0	0.209	0.209	0.209	0.250	0.232	0.234	0.234	0.250
0.5	0.235	0.236	0.235	0.250	0.263	0.263	0.263	0.250
1.0	0.262	0.262	0.260	0.250	0.292	0.292	0.290	0.250
		σ_{zz}				σ_{zz}		
−1.0	0.000	0.021	1.301	13.10	0.000	0.005	0.882	21.85
−0.5	0.000	0.036	2.131	21.65	0.000	0.009	1.438	36.10
0.0	0.000	0.073	3.335	35.75	0.000	0.016	2.237	59.60
0.5	0.000	0.130	5.055	58.90	0.000	0.028	3.364	98.20
1.0	0.000	0.201	7.565	97.05	0.000	0.032	4.989	161.7

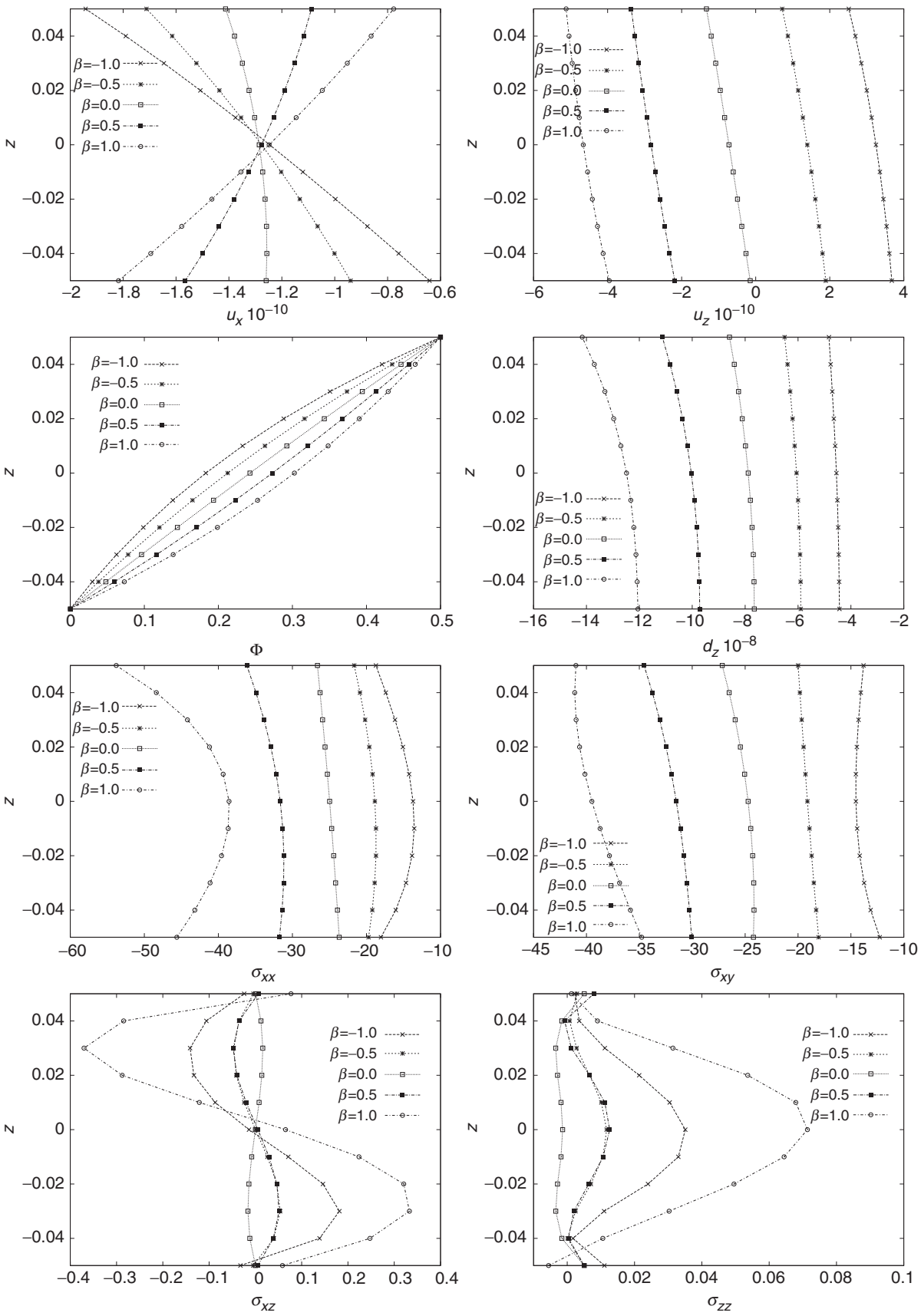

Figure 6. *Functionally graded piezoelectric plate with thickness $h = 0.1$. Actuator configuration, $N = 4$ model. Three-dimensional solution by Lu et al. (2006).*

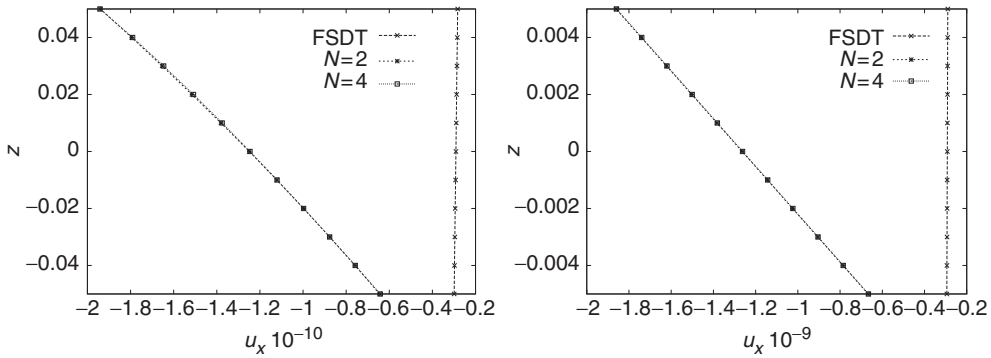

Figure 7. *Functionally graded piezoelectric plate with thickness h = 0.1 (left) and h = 0.01 (right). Actuator configuration, N = 4, N = 2, and FSDT models. Exponential $\beta = -1.0$.*

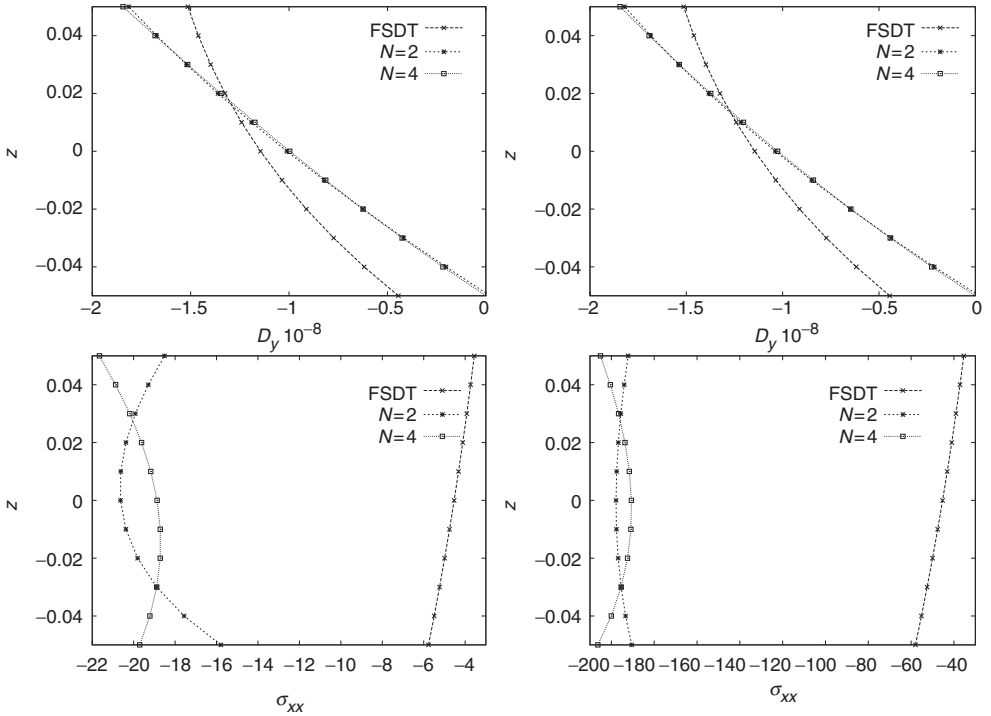

Figure 8. *Functionally graded piezoelectric plate with thickness h = 0.1 (left) and h = 0.01 (right). Actuator configuration, N = 4, N = 2, and FSDT models. Exponential $\beta = -0.5$.*

APPENDIX

To obtain the closed-form solution of the proposed fundamental nuclei, an harmonic form of the primary variables is supposed that corresponds to the simply supported boundary conditions for the plate:

$$
\begin{aligned}
u_x &= \bar{u}_x \cos(\alpha x)\sin(\beta y)\\
u_y &= \bar{u}_y \sin(\alpha x)\cos(\beta y)\\
u_z &= \bar{u}_z \sin(\alpha x)\sin(\beta y)\\
\Phi &= \bar{\Phi} \sin(\alpha x)\sin(\beta y)
\end{aligned}
$$

with $\alpha = (m\pi)/a$ and $\beta = (n\pi)/b$, where m and n are wavenumbers and a and b the in-plane plate dimensions. To obtain the closed form, transversely isotropic materials are considered, which means: $C_{16} = C_{26} = C_{63} = C_{36} = C_{45} = 0$ and $e_{25} = e_{14} = e_{36} = \varepsilon_{12} = 0$.

- $\boldsymbol{K}_{uu}^{k\tau sr}$

$$
\begin{aligned}
K_{uu_{11}} &= E^k_{\tau sr}(C^k_{11r}\alpha^2 + C^k_{66r}\beta^2) + E^k_{\tau_z s_z r}C^k_{55r}\\
K_{uu_{12}} &= E^k_{\tau sr}\alpha\beta(C^k_{12r} + C^k_{66r})\\
K_{uu_{13}} &= -E^k_{\tau s_z r}C^k_{13r}\alpha + E^k_{\tau_z sr}C^k_{55r}\alpha\\
K_{uu_{21}} &= E^k_{\tau sr}\alpha\beta(C^k_{12r} + C^k_{66r})\\
K_{uu_{22}} &= E^k_{\tau sr}(C^k_{22r}\beta^2 + C^k_{66r}\alpha^2) + E^k_{\tau_z s_z r}C^k_{44r}\\
K_{uu_{23}} &= -E^k_{\tau s_z r}\beta C^k_{23r} + E^k_{\tau_z sr}\beta C^k_{44r}\\
K_{uu_{31}} &= -E^k_{\tau_z sr}\alpha C^k_{13r} + E^k_{\tau s_z r}\alpha C^k_{55r}\\
K_{uu_{32}} &= -E^k_{\tau_z sr}\beta C^k_{23r} + E^k_{\tau s_z r}\beta C^k_{44r}\\
K_{uu_{33}} &= C^k_{33r}E^k_{\tau_z s_z r} + E^k_{\tau sr}(\alpha^2 C^k_{55r} + \beta^2 C^k_{44r})
\end{aligned}
$$

- $\boldsymbol{K}_{u\Phi}^{k\tau sr}$

$$
\begin{aligned}
K_{u\Phi_{11}} &= \alpha(E^k_{\tau_z sr} e^k_{15r} - E^k_{\tau s_z r} e^k_{31r}) \\
K_{u\Phi_{21}} &= \beta(E^k_{\tau_z sr} e^k_{24r} - E^k_{\tau s_z r} e^k_{32r}) \\
K_{u\Phi_{31}} &= E^k_{\tau sr}(\alpha^2 e^k_{15r} + \beta^2 e^k_{24r}) + E^k_{\tau_z s_z r} e^k_{33r}
\end{aligned}
$$

- $\boldsymbol{K}_{\Phi u}^{k\tau sr}$

$$
\begin{aligned}
K_{\Phi u_{11}} &= \alpha(-E^k_{\tau s_z r} e^k_{15r} + E^k_{\tau_z sr} e^k_{31r}) \\
K_{\Phi u_{12}} &= \beta(-E^k_{\tau s_z r} e^k_{24r} + E^k_{\tau_z sr} e^k_{32r}) \\
K_{\Phi u_{13}} &= E^k_{\tau sr}(-\alpha^2 e^k_{15r} - \beta^2 e^k_{24r}) - E^k_{\tau_z s_z r} e^k_{33r}
\end{aligned}
$$

- $\boldsymbol{K}_{\Phi\Phi}^{k\tau sr}$

$$
K_{\Phi\Phi_{11}} = E^k_{\tau sr}(\alpha^2 \varepsilon_{11r} + \beta^2 \varepsilon_{22r}) + \varepsilon_{33r} E^k_{\tau_z s_z r}\,.
$$

The meaning of integrals on z direction follows:

$$
\begin{aligned}
&\left(E^k_{\tau sr},\, E^k_{\tau_z sr},\, E^k_{\tau s_z r},\, E^k_{\tau_z s_z r}\right) \\
&= \int_{A_k} \left(F_\tau F_s F_r,\, \frac{\partial F_\tau}{\partial z} F_s F_r,\, F_\tau \frac{\partial F_s}{\partial z} F_r,\, \frac{\partial F_\tau}{\partial z}\frac{\partial F_s}{\partial z} F_r\right) \mathrm{d}z.
\end{aligned}
$$

REFERENCES

Almajid, A., Taya, M. and Hudnut, S. 2001. "Analysis of Out-of-plane Displacement and Stress Field in a Piezocomposite Plate with Functionally Graded Microstructure," *International Journal of Solids and Structures*, 38(19):3377–3391.

Ballhause, D., D'Ottavio, M., Kroplin, B. and Carrera, E. 2005. "A Unified Formulation to Assess Multilayered Theories for Piezoelectric Plates," *Computers and Structures*, 83(15–16):1217–1235.

Bhangale, R.K. and Ganesan, N. 2006. "Static Analysis of Simply Supported Functionally Graded and Layered Magneto-electro-elastic Plates," *International Journal of Solids and Structures*, 43(10):3230–3253.

Brischetto, S. and Carrera, E. 2008. "Advanced Mixed Theories for Bending Analysis of Functionally Graded Plates," *Computers and Structures*, available online.

Brischetto, S., Leetsch, R., Carrera, E., Wallmersperger, T. and Kroplin, B. 2008. "Thermo-mechanical Bending of Functionally Graded Plates," *Journal of Thermal Stresses*, 31(3):286–308.

Carrera, E., 1995. "A Class of Two Dimensional Theories for Multilayered Plates Analysis," *Accademia delle Scienze di Torino, Mem. Sci. Fis.*, 19–20:49–87.

Carrera, E. 2003. "Theories and Finite Elements for Multilayered Plates and Shells: A Unified Compact Formulation with Numerical Assessment and Benchmarks," *Archivies of Computational Methods in Engineering*, 10(3):215–296.

Carrera, E. and Boscolo. M. 2007. "Classical and Mixed Finite Elements for Static and Dynamic Analysis of Piezoelectric Plates ," *International Journal for Numerical Methods in Engineering*, 70(10):1135–1181.

Carrera, E. and Brischetto, S. 2007. "Piezoelectric Shells Theories with a Priori Continuous Transverse Electromechanical Variables," *Journal of Mechanics of Materials and Structures*, 2(2):377–399.

Carrera, E., Brischetto, S. and Robaldo, A. 2008. "Variable Kinematic Model for the Analysis of Functionally Graded Material Plates," *AIAA Journal*, 46(1):194–203.

Chen, W.Q. and Ding, H.J. 2002. "On Free Vibration of a Functionally Graded Piezoelectric Rectangular Plate," *Acta Mechanica*, 153(3–4):207–216.

Chen, X.L., Zhao, Z.Y. and Liew, K.M. 2008. "Stability of Piezoelectric FGM Rectangular Plates Subjected to Non-uniformly Distributed Load, Heat and Voltage," *Advances in Engineering Software*, 39(2):121–131.

Dai, K.Y., Liu, G.R., Han, X. and Lim, K.M. 2005. "Thermomechanical Analysis of Functionally Graded Material (FGM) Plates using Element-free Galerkin Method," *Computers and Structures*, 83(17–18):1487–1502.

He, X.Q., Ng, T.Y., Sivashanker, S. and Liew, K.M. 2001. "Active Control of FGM Plates with Integrated Piezoelectric Sensors and Actuators," *International Journal of Solids and Structures*, 38(9):1641–1655.

He, X., Wang, J.-S. and Qin, Q.-H. 2007. "Saint-Venant Decay Analysis of FGPM Laminates and Dissimilar Piezoelectric Laminates," *Mechanics of Materials*, 39(12):1053–1065.

Joshi, S., Mukherjee, A. and Schmauder, S. 2003. "Exact Solutions for Characterization of Electro-elastically Graded Materials," *Computational Materials Science*, 28(3–4):548–555.

Li, X.Y., Ding, H.J. and Chen, W.Q. 2008. "Three-dimensional Analytical Solution for Functionally Graded Magneto-electro-elastic Circular Plates Subjected to Uniform Load," *Composite Structures*, 83(4):381–390.

Liew, K.M., He, X.Q. and Ray, T. 2004. "On the Use of Computational Intelligence in the Optimal Shape Control of Functionally Graded Smart Plates," *Computational Methods in Applied Mechanics and Engineering*, 193(42–44):4475–4492.

Lu, P., Lee, H.P. and Lu, C. 2005. "An Exact Solution for Functionally Graded Piezoelectric Laminates in Cylindrical Bending," *International Journal of Mechanical Sciences*, 47(3):437–458.

Lu, P., Lee, H.P. and Lu, C. 2006. "Exact Solutions for Simply Supported Functionally Graded Piezoelectric Laminates by Stroh-like Formalism," *Composite Structures*, 72(3):352–363.

Ootao, Y. and Tanigawa, Y. 2000. "Three-dimensional Transient Piezothermoelasticity in Functionally Graded Rectangular Plate Bonded to a Piezoelectric Plate," *International Journal of Solids and Structures*, 37(32):4377–4401.

Pan, E. and Han, F. 2005a. "Exact Solution for Functionally Graded and Layered Magneto-electro-elastic Plates," *International Journal of Engineering Science*, 43(3–4):321–339.

Pan, E. and Han, F. 2005b. "Green's Functions for Transversely Isotropic Piezoelectric Functionally Graded Multilayered Half Spaces," *International Journal of Solids and Structures*, 42(11–12):3207–3233.

Ray, M.C. and Sachade, H.M. 2006. "Finite Element Analysis of Smart Functionally Graded Plates," *International Journal of Solids and Structures*, 43(18–19):5468–5484.

Takagi, K., Li, J.-F., Yokoyama, S. and Watanabe, R. 2003. "Fabrication and Evaluation of PZT/Pt Piezoelectric Composites and Functionally Graded Actuators," *Journal of the European Ceramic Society*, 23(10):1577–1583.

Wu, X.-H., Shen, Y.-P. and Chen, C. 2002. "A High Order Theory for Functionally Graded Piezoelectric Shells," *International Journal of Solids and Structures*, 39(20):5325–5344.

Zhong, Z. and Shang, E.T. 2003. "Three-dimensional Exact Analysis of a Simply Supported Functionally Gradient Piezoelectric Plate," *International Journal of Solids and Structures*, 40(20):5335–5352.